# NASA TECHNICAL NOTE

NASA TN D-6922

# PERFORMANCE AND OPERATING CHARACTERISTICS OF THE ARC-DRIVEN LANGLEY 6-INCH SHOCK TUBE

*by John E. Nealy*

*Langley Research Center*
*Hampton, Va. 23365*

| 1. Report No.<br>NASA TN D-6922 | 2. Government Accession No. | 3. Recipient's Catalog No. |
|---|---|---|
| 4. Title and Subtitle<br><br>PERFORMANCE AND OPERATING CHARACTERISTICS<br>OF THE ARC-DRIVEN LANGLEY 6-INCH SHOCK TUBE | | 5. Report Date<br>August 1972 |
| | | 6. Performing Organization Code |
| 7. Author(s)<br><br>John E. Nealy | | 8. Performing Organization Report No.<br>L-8312 |
| | | 10. Work Unit No.<br>117-07-04-09 |
| 9. Performing Organization Name and Address<br><br>NASA Langley Research Center<br>Hampton, Va. 23365 | | 11. Contract or Grant No. |
| | | 13. Type of Report and Period Covered<br>Technical Note |
| 12. Sponsoring Agency Name and Address<br>National Aeronautics and Space Administration<br>Washington, D.C. 20546 | | 14. Sponsoring Agency Code |

15. Supplementary Notes

16. Abstract

    Performance characteristics for the arc-driven Langley 6-inch shock tube have been determined for driver energies from 0.62 to 5 MJ. Voltage, current, and pressure histories of the arc driver have been recorded, and driver efficiencies have been determined from measured shock velocities. Time-resolved spectra for test gases of air, carbon monoxide, xenon, and a mixture of 80 percent helium and 20 percent hydrogen are presented.

| 17. Key Words (Suggested by Author(s))<br><br>Shock tube<br>Electric arc | 18. Distribution Statement<br><br>Unclassified — Unlimited |
|---|---|
| 19. Security Classif. (of this report)<br>Unclassified | 20. Security Classif. (of this page)<br>Unclassified |

| 19. Security Classif. (of this report) | 20. Security Classif. (of this page) | 21. No. of Pages | 22. Price* |
|---|---|---|---|
| Unclassified | Unclassified | 27 | $3.00 |

# PERFORMANCE AND OPERATING CHARACTERISTICS OF THE
# ARC-DRIVEN LANGLEY 6-INCH SHOCK TUBE

By John E. Nealy
Langley Research Center

## SUMMARY

Performance characteristics for the arc-driven Langley 6-inch shock tube have been determined for driver energies from 0.62 to 5 MJ. Voltage, current, and pressure histories of the arc-driver properties have been recorded, and driver efficiencies have been determined from measured shock velocities. Time-resolved spectra for test gases of air, carbon monoxide, xenon, and a mixture of 80 percent helium and 20 percent hydrogen are presented. The capability of the facility for use in research studies of high-temperature gas radiation and chemistry has been established.

## INTRODUCTION

Use of the arc-driven shock tube as a means for producing shock-heated gas samples is well documented. (See, for example, refs. 1, 2, and 3.) Planetary entry velocities for Venus, Jupiter, and Saturn fall in the 10- to 60-km/sec range, and high-performance impulse facilities appear to offer the best approach for studying the high-temperature gas properties in shock layers about vehicles in this speed regime. The arc-driven Langley 6-inch shock tube has by far the most driver energy available of existing arc-driven facilities. At this time little experience exists in heating helium by discharges of several million joules with consequent peak currents upwards of a million amperes. Maintaining a relatively high efficiency is essential to the effective utilization of this large energy. Therefore, particular emphasis has been placed on the behavior of the driver during the series of runs reported herein. The more pertinent parameters associated with the electric discharge have been measured, for example, time variation of voltage and current during discharge and, in some instances, the driver-pressure variation during and immediately after discharge.

The performance characteristics presented are primarily for air as the test gas, but these may be used to indicate expected performance for other gas mixtures. The measured shock velocity has been used to determine driver efficiency, that is, the effective transfer of arc energy to the initially cold helium driver gas. In addition to shock-velocity measurements in the test gas, pressures, luminosity profiles, and time-resolved spectral properties have also been investigated.

## SYMBOLS

$H_\beta, H_\gamma, H_\delta$    lines of the Balmer series of the hydrogen spectrum

$I$    current

$p_1$    initial test-gas pressure

$p_{max}$    maximum design pressure

$T_{2,eq}$    computed equilibrium temperature behind normal shock

$t$    time

$V_s$    shock velocity

## GENERAL DESCRIPTION

The shock tube basically consists of three stainless steel sections: a 0.61-meter-long, 0.15-meter-diameter driver chamber, a 15.2-meter-long, 0.15-meter-diameter driven-tube section, and a 3.05-meter-long, 0.305-meter-diameter dump tank. Four-petal stainless steel diaphragms varying in thickness from 0.47 to 0.94 cm are used. When the diaphragm breaks, the petals open into a square-to-round insert section. A detailed schematic drawing depicting the relative locations of the various components is presented in figure 1. Two test sections are available; these can be used at the flanged ends of any of the four driven-tube sections. These test sections are equipped with boundary-layer splitter plates and 0.25-cm-thick by 2.5-cm-diameter cylindrical window ports. A photograph of the window-insert assembly with splitter plate is shown in figure 2. When two test sections are used, the splitter plates are installed at the second test section. Additional instrumentation ports are placed at 13 locations along the driven tube.

The capacitor bank for the shock tube consists of two racks of capacitors, each individual capacitor having 43-$\mu$F capacitance and rated at 12 kV. The total capacitance of each rack is about 0.035 farad. Both racks charged to the maximum 12 kV operating voltage give the total bank an energy of 5 MJ. Each rack of capacitors is connected by 80 coaxial cables to a collector ring. The two collector rings may then be mounted in parallel and deliver the bank energy into the arc chamber, or a single rack may be used alone. A separate bank of 10 capacitors of the same type as are in the main bank is used to explode a trigger wire and initiate the main arc.

A photograph of the shock-tube driver is shown in figure 3. The driver chamber is shown in its open position; the square end of the square-to-round insert section at the diaphragm location is also visible. A photograph of the shock-tube driven section is shown in figure 4. An f/6.3 grating spectrograph equipped with rotating drum camera is in place at the second test section. This instrument was used in obtaining the time-resolved spectra described later in this paper.

The main high-voltage electrode is made of zirconium-copper alloy and is doughnut shaped, with the trigger electrode at its center and insulated from it. A detailed drawing of the shock-tube driver chamber is presented in figure 5. Before each run, a trigger wire is strung from the nose of the trigger electrode to the ground electrode approximately 50 cm away from it. The trigger wire is isolated from its bank by an open switch located near the bank. The run is initiated by closing this switch. It was found that in order to initiate main-arc breakdown using less than 10 kV, it is necessary to attach a small piano-wire leader to the trigger electrode so that the trigger wire then comes to within about 1 cm of the main electrode. This means of trigger-wire installation has given reliable arc initiation using voltages as low as 7 kV. So far the types of trigger wires used successfully have been a 0.052-cm-diameter fuse wire and a 0.012-cm-diameter tungsten wire. The tungsten wire is favored because of its ease in handling.

Another common method of triggering is that of pulling a wire from one main electrode to the other. (See, for example, refs. 2 and 3.) Perhaps one advantage of the present method is that the trigger bank may be operated at a different voltage than the main bank, possibly allowing easier arc initiation at lower voltage gradients. However, during the present tests, the initial trigger-bank voltage was the same as that for the main bank.

Several runs were made for which the ground electrode was a cylindrical zirconium-copper ring mounted flush against the inner wall of the driver chamber. It was felt that a ground electrode centered in the driver chamber by means of a spider support would provide easier arc initiation and more uniform heating of the driver gas. Such an alteration would slightly shorten the arc travel distance and maintain it more nearly in the central region of the cylindrical driver chamber. This new configuration was implemented midway through the shakedown program, with the ground electrode made of silver-copper alloy and hemispherically shaped. While somewhat easier arc initiation was evidenced, no significant change in the electrical behavior or efficiency of the driver resulted from this alteration. Inspection of the spider-supported ground electrode after several runs showed that the arc was not strictly confined to the silver-copper hemisphere but also attached itself to the spider structure. Apparently no significant damage or erosion occurred as a result of this behavior.

A further problem which had to be resolved was that of which diaphragm was best suited for operation at a particular driver energy. It has been found that for capacitor-bank energies between 0.6 and 1.1 MJ, a 0.47-cm-thick stainless steel diaphragm with

groove depth of 0.23 cm is adequate.  For energies between 1.1 and 1.75 MJ, a 0.63-cm-thick diaphragm with a 0.25-cm-deep groove has been used satisfactorily.  A 0.94-cm-thick diaphragm with 0.44-cm groove depth has been used for bank energies between 1.75 and 5 MJ.

For driver energies above 1.7 MJ, it was necessary to provide replaceable energy-absorbing soft-metal cushions in the walls of the square-to-round insert section at the four locations of diaphragm-tab impact.  This prevented loss of tips of diaphragm tabs due to shear forces.  Pads made of either 0.64-cm-thick soft aluminum or brass have been found to be suitable.  This procedure has been successfully employed previously at the Ames arc-driven shock-tube facility (ref. 2) and has been equally successful in application at this facility.

## ARC-HEATED-DRIVER MEASUREMENTS

In order to properly evaluate the behavior of the driver, the time variation of the voltage and current during the arc discharge must be monitored.  A piezoelectric pressure gage has been used to measure pressure in the driver chamber during the discharge.  A schematic drawing of the instrumentation layout used in measuring these parameters is shown in figure 6.  The various components involved in making the measurements are identified on the sketch.  Sample oscilloscope records using this arrangement are shown in figure 7 for a run using one capacitor rack at 7.5 kV and a driver chamber containing helium at an initial pressure of 200 $N/cm^2$.

Many of the driver pressure histories during arc discharge were distorted, apparently being disturbed by electromagnetic pickup or circulating ground currents.  Some runs, however, such as the example in figure 7, appeared to be free of major disturbances, and the records were assumed to be a correct history of the pressure at the measurement location, which is on the driver wall about 4.5 cm from the diaphragm.  Typically, the pressure increased rapidly at about the time of peak current, a strong shock or compression wave generated by the arc being indicated.  Often a double pressure peak was observed, which is only slightly evident in the record in figure 7.  It can be seen in this figure that peak pressure was measured to be around 5500 $N/cm^2$; a calculated driver pressure of 6130 $N/cm^2$ results when assuming 100-percent efficiency of arc-energy transfer.  The 300 to 400 $\mu$sec that it takes for the pressure to decay to a low value is indicative of the opening time of the diaphragm.

A number of oscilloscope records of voltage and current histories were used in the computation of arc conductance and power histories.  Figures 8 and 9 illustrate the reduced records for one- and two-rack operation at 9 kV and at 12 kV.  The voltage discharge appears to be almost critically damped for the 9-kV one-rack run and underdamped

for the 12-kV runs. Arc-conductance calculations from the digitized records generally fall in the 200- to 600-mho range and exhibit considerable scatter without showing distinct trends.

## SHOCK-TUBE PERFORMANCE

### Velocity Measurements

The most important measure of shock-tube performance is the shock velocity resulting from a given set of initial conditions. In this facility several methods of determining shock velocity are available so that redundancy may be acheived in making this measurement. This is fortunate since no one method has proved completely satisfactory over all speed ranges. Aircraft spark plugs used as ionization probes have been heavily relied upon. Their signal at shock passage is fed to a rack of megahertz counters and also to a raster-oscilloscope combination. This method of shock location has been reliable for shock waves in a speed range where precursor ionization is insignificant. For shock waves in air at speeds greater than about 11 km/sec, additional methods of shock-velocity measurement had to be employed.

A microwave generator operating at a frequency of 1.3 GHz was used to inject a signal to a straight-probe antenna located at a far downstream instrumentation port, approximately 16 meters from the diaphragm. The antenna itself was a cylindrical steel rod 0.63 cm in diameter extending 3.8 cm into the driven tube. The signal reflected from the moving ionization front interferes with the radiated carrier signal, and the corresponding amplitude modulation of the carrier frequency is recorded on a rotating-drum camera used with a dual-beam oscilloscope. This procedure is not uncommon and a good evaluation of the relative merits and limitations may be found in references 4 and 5. The existence of heavy precursor ionization for strong shock waves rendered the microwave signal unsuitable for straightforward interpretation. The microwave system could be utilized at only slightly higher shock velocities than the ionization probes. However, when speed measurements using microwaves were obtained, the information was considerably detailed, since the signal peaks provided shock-position points at 23-cm increments until the time of shock passage at the antenna location. In figure 10 the behavior of a microwave signal under conditions of strong precursor ionization is compared with that obtained for a relatively low-speed run with negligible effect from precursor ionization.

Speed measurements under conditions of strong precursor ionization were made from photomultiplier and piezoelectric pressure-gage signals. For future projects requiring shock waves in this high-speed range, a system of photodetectors will be used in place of the ionization probes, and their output signals fed to the megahertz counters and raster-oscilloscope combination. Solid-state photodiodes are favored because of their low cost and simple auxiliary electronics. Such a photodiode system is presently being assembled.

A plot of measured shock velocity as a function of initial capacitor-bank energy is shown in figure 11 for initial driven pressures of 1, 5, and 20 torr (1 torr = 0.0133 $N/cm^2$) and over a range of driver energies of 0.62 to 5 MJ. Shock velocities were measured between 6 and 21 km/sec. Most shock velocities were measured about 16 meters from the diaphragm location, close to the last test section. For some of the high-speed runs, the velocity had to be determined from pressure gages and phototubes at stations about 8 meters from the diaphragm. All runs were made with the driver gas, helium, at an initial pressure of about 200 $N/cm^2$. In addition to the shock-velocity data, the computed performance of a 50-percent-efficient driver in air with an initial pressure of 1 torr is presented. This value for efficiency was used as a guideline for expected performance in design predictions. It is apparent that below a capacitor-bank energy of 2.5 MJ, the 1-torr data fall consistently above the 50-percent-efficiency curve.

In a few instances, test gases other than air have been used. For the single 5-MJ run, a mixture of 80 percent helium and 20 percent hydrogen was used at an initial pressure of 1 torr. A shock velocity of 20.8 km/sec was measured for the corresponding driver-energy density of 464 $J/cm^3$. Reference 3 shows that for similar initial conditions, a driver-energy density of 820 $J/cm^3$ produced a shock velocity of 21.5 km/sec at a distance of 3.7 meters from the diaphragm. This shock had attenuated to 17.5 km/sec at a distance of 10.7 meters. Thus, a comparable shock velocity was achieved in reference 3 with much less total energy but at the sacrifice of driver efficiency. The very high energy density was achieved in those tests by using a very small driver volume (350 $cm^3$).

## Driver-Efficiency Determination

From the measured shock velocity from each run and a knowledge of the initial amount of driver energy available, a driver efficiency was determined by calculating the driver energy necessary to produce the shock wave and dividing the result by the total electrical energy initially existing. A plot showing the results of this procedure is given in figure 12. Although a relatively large scatter of the data is evident, the calculated efficiencies obviously decrease with increasing available driver energy above about 1 MJ. Computed driver efficiencies are generally over 50 percent for driver energies up to 2.5 MJ and below 50 percent at higher energies. The usual assumption was made that thermodynamic equilibrium existed behind the shock wave, and the resultant pressures and velocities were matched to equivalent pressures and velocities of the unsteady isentropic expansion of the helium driver gas. It was also assumed that the driver gas was thermally perfect and uniformly heated in a constant-area chamber. The insertion of the spider-supported ground electrode in the driver chamber causes an area reduction of about 20 percent. The behavior of this area change as a throat restriction has been considered and found to have a negligibly small effect on the computed efficiencies.

Since only partial shock-velocity data were available on some runs, some of the scatter in the efficiency data may be due to determining the shock velocity at different distances from the diaphragm, and thereby including less or more attenuation effects. Other factors which might contribute to the data scatter are presently speculative; some which possibly are important include variations in diaphragm-opening characteristics and varying arc configuration.

The efficiencies for the few two-rack runs are significantly lower than those for the single-rack runs. This lower efficiency is assumed to be the result of the longer discharge times observed for two-rack runs. The voltage-versus-time oscilloscope records were examined for all runs. Those showing no oscillation were applied to the case of a critically damped series R-L-C (resistance-inductance-capacitance) circuit, and an inductance value was estimated. Such an analysis gives the inductance as $0.614 \pm 0.120$ $\mu$H.

If it is further assumed that the observed underdamped discharges occur as a result of a major reduction in the effective arc resistance, discharge frequencies for the one- and two-rack configurations may be computed and compared with the measured values. (All two-rack runs show oscillatory-voltage histories.) Some justification for this assumption is that theoretical inductance calculations indicate that very little change in circuit inductance occurs when two capacitor racks are used instead of one. For the two-rack configuration, the capacitance is doubled.

The frequency for one capacitor rack computed from the value of inductance given previously is $1.10 \pm 0.11$ kHz, whereas the measured value is $1.07 \pm 0.02$ kHz. For two-rack operation the computed value is $0.776 \pm 0.078$ kHz, and the measured value is $0.686 \pm 0.017$ kHz. Thus, a discharge time for two racks exceeds that for one rack by about 50 percent. It is not entirely unexpected that lower discharge frequency results in decreased efficiency since more time may be available for nonadiabatic effects to occur.

## Flow-Diagnostic Observations

The ultimate use of a high-performance shock tube as a research tool is in the study of high-temperature gas radiation and chemistry. The evaluation of the future utilization of this facility in such research efforts has been given an important place in the shakedown program. Several test gases have been examined as candidates for shock-tube studies, and calculations of equilibrium conditions behind normal shocks for these gases have been made using the program of reference 6.

Figure 13 shows the computed variation of equilibrium temperature behind normal shock waves for the four test gases chosen for the spectroscopic observations at an initial pressure of 1 torr. While the calculated equilibrium temperature gives some indication of the state of the shocked gas, there is a relaxation zone behind the shock where gas temperatures are generally higher. Calculation of equilibrium properties for xenon

presented some problems, since insufficient partition-function data exist for the fourth and fifth ionization stages of xenon (ref. 7). Isoelectronic comparisons, extrapolations, and crossplots were used to estimate the ionization potentials and lower lying electronic state energies of Xe V and Xe VI. In a similar type of extrapolation, reference 8 gives a value of 89 eV as the ionization potential of Xe VI, which differs considerably from the value deduced here. However, for the speed range given in figure 13, the computed equilibrium temperatures are not significantly affected when a value of 64 eV is used as the ionization potential of Xe VI. The values used in the calculations of equilibrium properties are given in the following table:

| Element | Ionization potential, eV | Energy level, per cm | Degeneracy |
|---------|--------------------------|----------------------|------------|
| Xe V | 56 | 0 | 1 |
| | | 514 | 3 |
| | | 1 403 | 5 |
| | | 14 409 | 5 |
| | | 34 070 | 1 |
| | | 107 601 | 15 |
| Xe VI | 64 | 0 | 2 |
| | | 1 408 | 4 |
| | | 81 184 | 2 |
| | | 81 692 | 4 |
| | | 82 488 | 6 |
| | | 106 893 | 4 |
| | | 106 981 | 6 |

Time-resolved spectra were obtained from runs into the various test gases using an f/6.3 grating spectrograph equipped with an air-driven rotating-drum camera as described in reference 9. In order to minimize boundary-layer effects and give increased observation time of the heated gas sample, the window-insert with splitter-plate assembly was employed.

Figure 14 shows the test portion of the drum-camera records and a densitometer trace, which has the same wavelength scale as the spectrum photograph. Identification of some of the important radiating species in the test gases is also given in the figures. Wavelengths were identified with the aid of references 10 and 11. The first burst of radiation for each case is immediately recognizable as characteristic of the particular test gas. The strong-line radiation appearing at later times in the flow are metallic impurities in the arc-heated driver gas. Iron, copper, chromium, and silver are the most prominent of the impurity radiators.

No sharp definition of test time can be obtained from the drum-camera spectra because of loss of time resolution due to the finite-slit height (1 mm) of the spectrograph. Relatively clean flow occurs for 10 to 15 $\mu$sec for the air and carbon monoxide test gases, considerably longer for the helium-hydrogen test gas, while for xenon the test time is too short to be observed on the spectrogram.

The $H_\beta$ line at 4861 Å observed in the air spectrum occurs as a result of approximately 2-percent water vapor in the initial test gas due to natural humidity. (Room air was used for most of the shakedown runs.) The corresponding equilibrium calculation for this run was performed including this initial water vapor, and it was found that practically all the hydrogen in the water molecule was converted to free hydrogen atoms behind the normal shock.

## CONCLUDING REMARKS

The arc-driven Langley 6-inch shock tube has been shown to be an operational facility capable of producing strong shock waves in various gas mixtures. Operational procedures and instrumentation techniques have been established so that research studies of high-temperature gas radiation and chemistry may be initiated. The facility has been operated at a peak driver energy of 5 MJ. Computed driver efficiencies are generally over 50 percent for driver energies up to 2.5 MJ and below 50 percent at higher energies. Shock velocities have been measured between 6 and 21 km/sec.

One of the most interesting developments to arise during the course of the shakedown program is that of the strong precursor ionization in front of very high-speed shock waves. Much work is yet to be done in order to define the properties of this phenomenon.

As research projects in this facility ensue, monitoring of the arc-driver properties of the facility should continue using the proven techniques described herein. An accumulation of arc-driver data should be useful in determining the important parameters involved in driver-chamber energy transfer.

Langley Research Center,
National Aeronautics and Space Administration,
Hampton, Va., June 23, 1972.

# REFERENCES

1. Camm, John C.; and Rose, Peter H.:   Electric Shock Tube for High Velocity Simulation. AFCRL-62-568, U.S. Air Force, July 1962.

2. Dannenberg, Robert E.; and Silva, Anthony F.:   Exploding Wire Initiation and Electrical Operation of a 40-kV System for Arc-Heated Drivers up to 10 Feet Long.   NASA TN D-5126, 1969.

3. Menard, W. A.:   A Higher Performance Electric-Arc-Driven Shock Tube.   JPL Quart. Tech. Rev., vol. 1, no. 1, Apr. 1971, pp. 17-28.

4. Hill, R. J.:   Anomalous Shock Velocity Measurements in Argon Using Microwaves. Phys. Fluids, vol. 7, pt. I, no. 11, Nov. 1964, pp. 1865-1866.

5. Koch, B.; and König, M.:   Digital Measurements of the Speed Variations of Shock Waves by Means of Microwaves.   Phys. Fluids, Suppl. I, vol. 12, pt. II, no. 5, May 1969, pp. I-144 – I-146.

6. Grose, William L.; Nealy, John E.; and Kemper, Jane T.:   A Digital Computer Program for Calculating the Performance of Single- or Multiple-Diaphragm Shock Tubes for Arbitrary Equilibrium Real Gas Mixtures.   NASA TN D-4802, 1968.

7. Crawford, Keith Eugene:   A Method of Calculating Equilibrium States Behind Incident and Reflected Shock Waves in Ionizing Monatomic Gases.   M.S. Thesis, Ohio State Univ., 1969.

8. Finkelnburg, W.; and Humbach, W.:   Ionisierungsenergien von Atomen und Atomionen. Die Naturwissenschaften, Jg. 42, Heft 2, 1955, pp. 35-37.

9. Mahugh, R. A.:   Adapting the Jarrell-Ash Model 75 Spectrograph for Time-Resolved Spectroscopy.   Appl. Opt., vol. 5, no. 12, Dec. 1966, pp. 1967-1969.

10. Striganov, A. R.; and Sventitskii, N. S.:   Tables of Spectral Lines of Neutral and Ionized Atoms.   IFI/Plenum Data Corp., 1968.

11. Meggers, William F.; Corliss, Charles H.; and Scribner, Bourdon F.:   Tables of Spectral-Line Intensities.   NBS Monogr. 32, Pt. I, U.S. Dep. Com., Dec. 29, 1961.

Two collector rings

Driver chamber

$(p_{max} = 30\ 000\ N/cm^2)$

Anchor tube

$(p_{max} = 10\ 000\ N/cm^2)$

Evacuation valve

$(p_{max} = 3330\ N/cm^2)$

Driven tubes-
four sections, 3.05 m long
$(p_{max} = 3330\ N/cm2)$

Test sections

$(p_{max} = 3330\ N/cm^2)$

Dump tank

$(p_{max} = 667\ N/cm^2)$
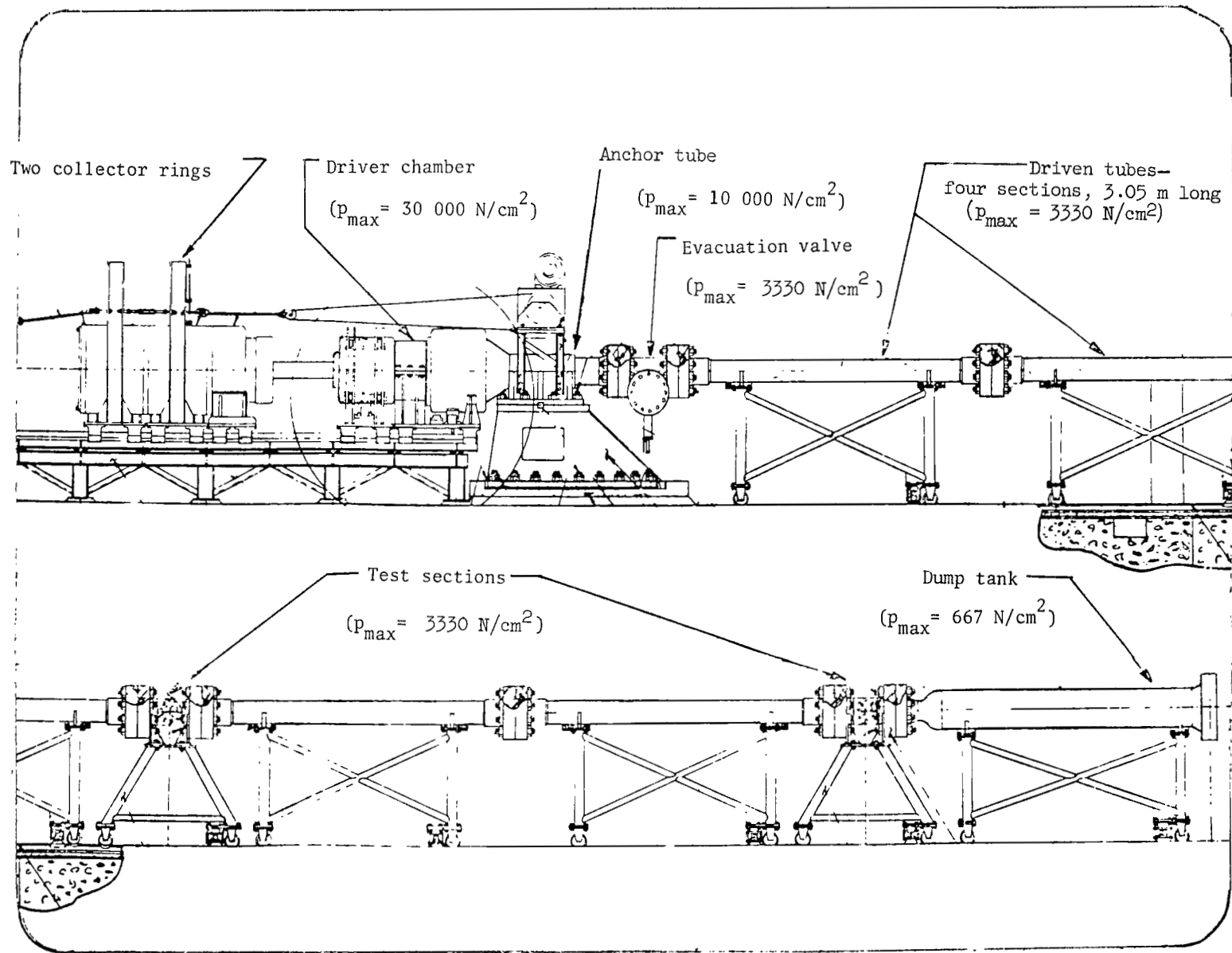
Figure 1.- Schematic drawing of the arc-driven Langley 6-inch shock tube of the hot gas radiation research facility.
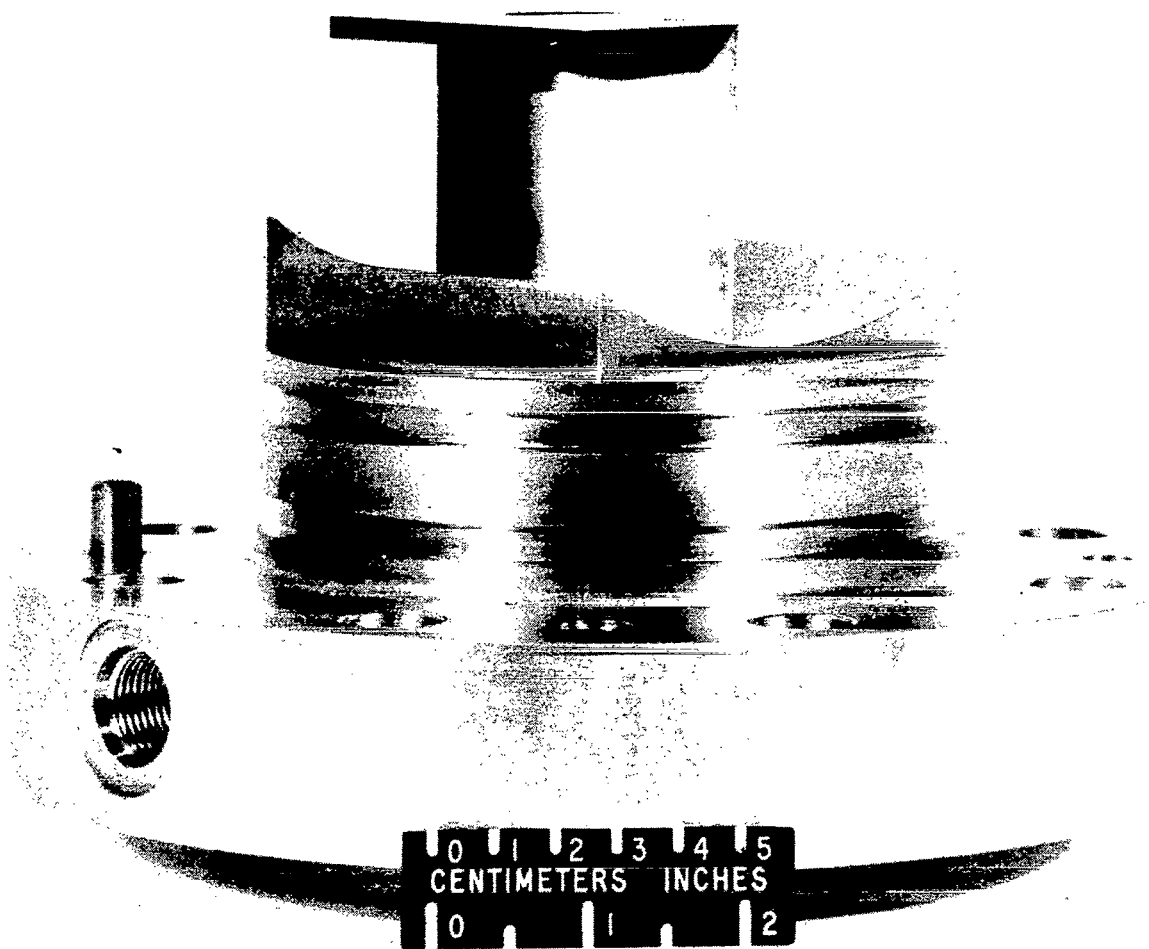
L-72-2451

Figure 2.- Test-section window insert showing splitter-plate assembly.
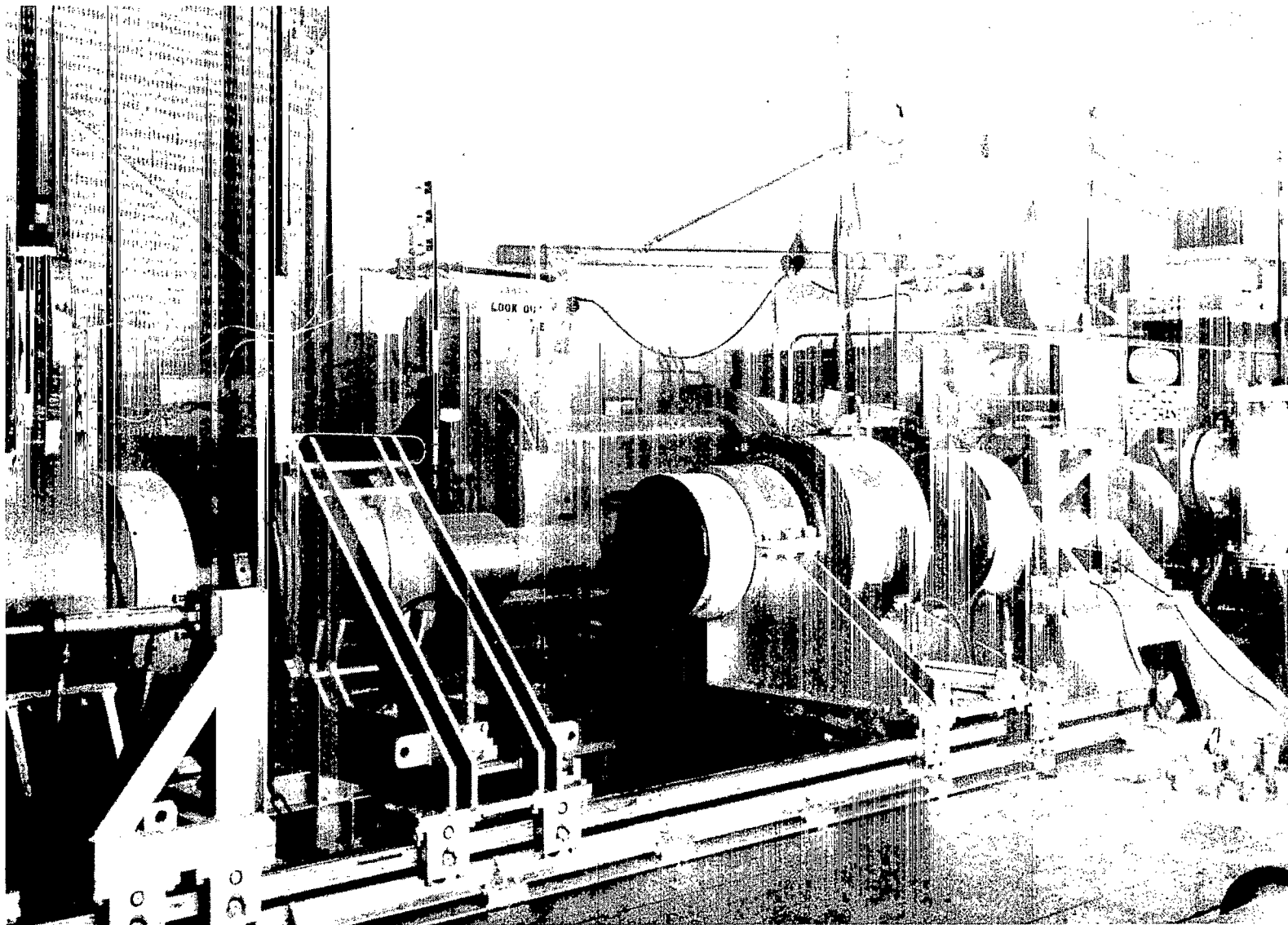
L-72-2452

Figure 3.- Shock-tube driver in open position.
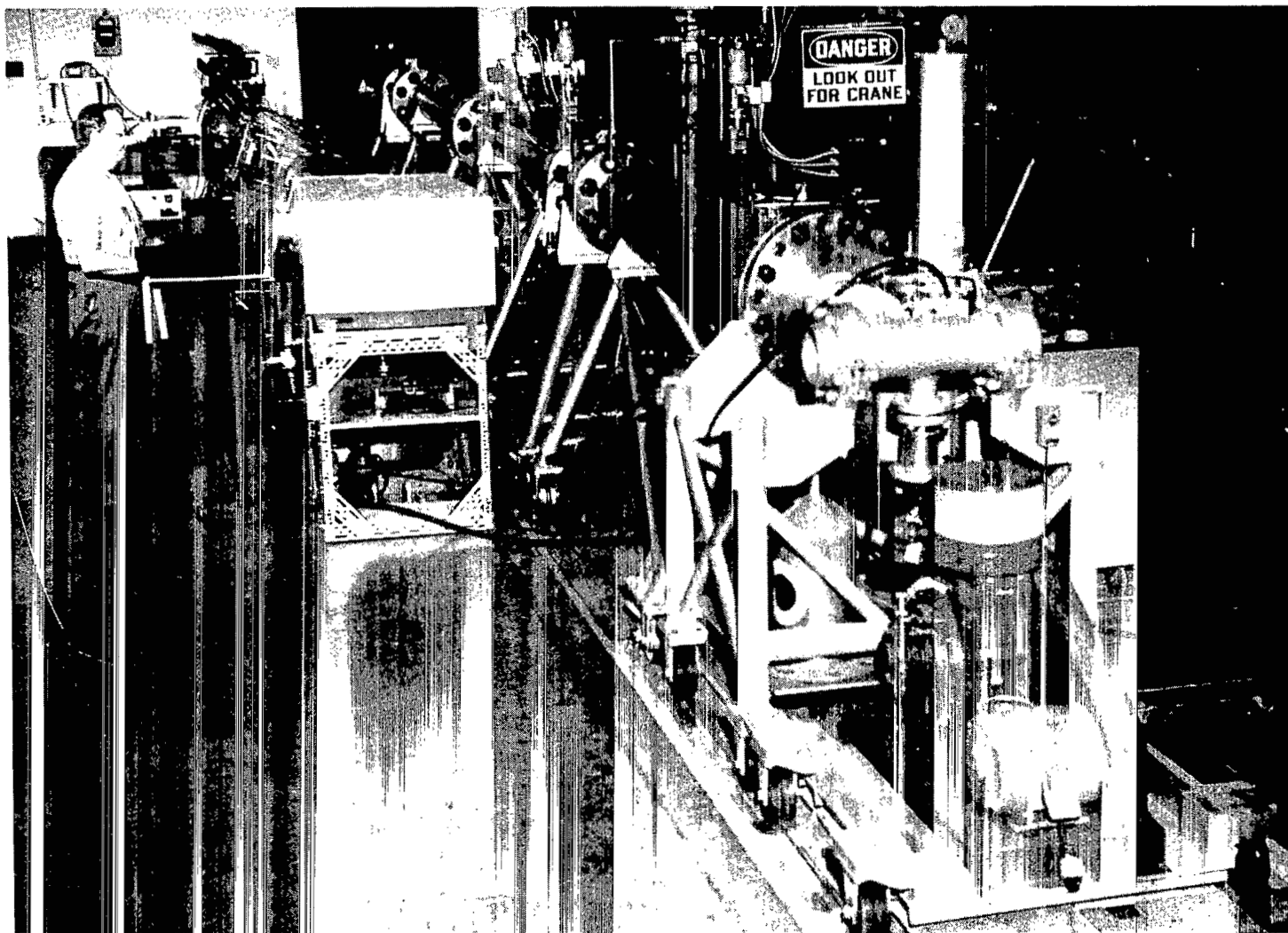
L-72-2453

Figure 4.- Shock-tube driven section with drum-camera spectrograph at second test section.

Main high-voltage electrode

Ground electrode with spider support (modification)

Insulator

Trigger electrode

Ground electrode

Diaphragm

Driver chamber
(0.61 m long and 0.15 m in diam.)

Square-to-round insert section
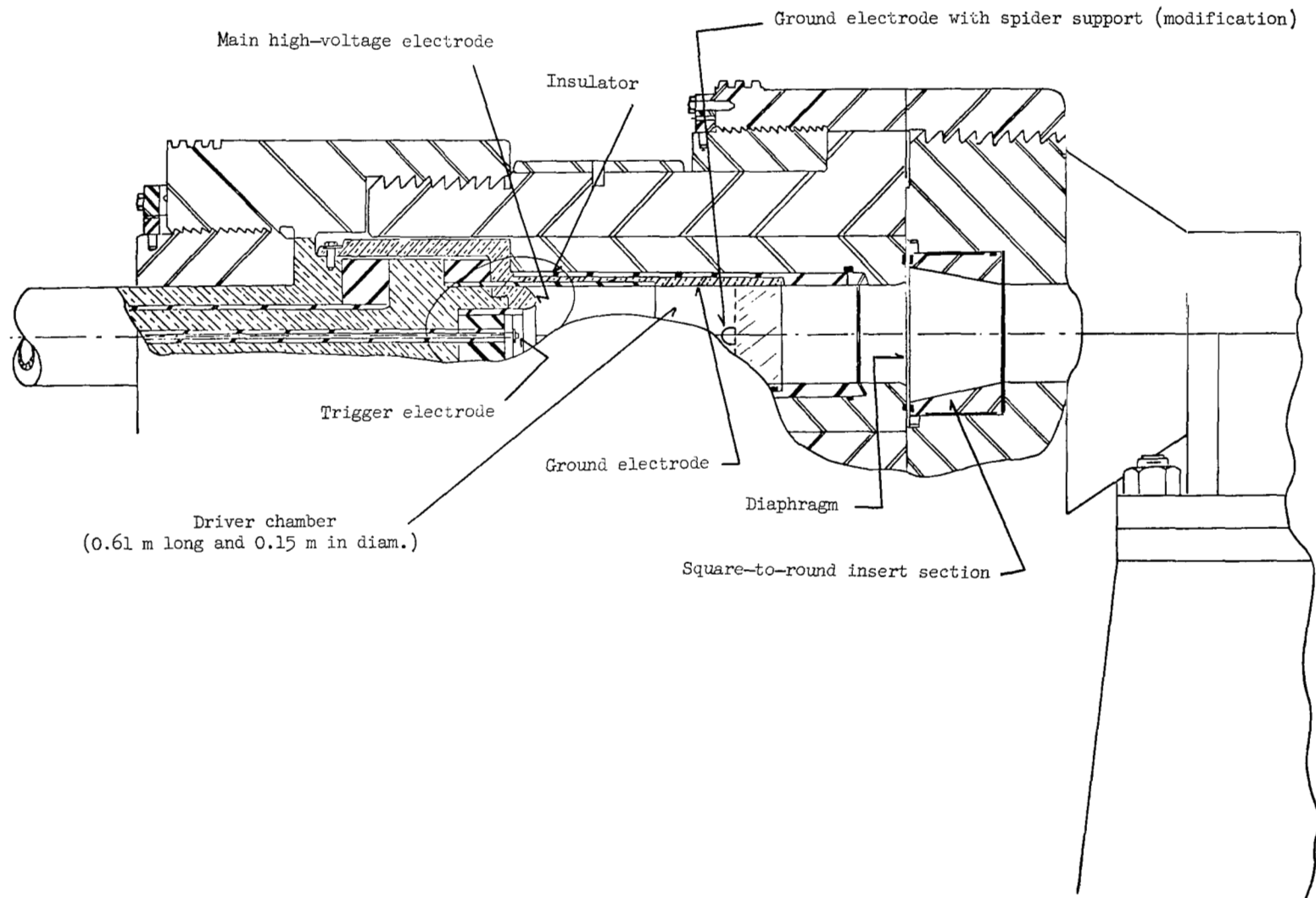
Figure 5.- Details of the shock-tube driver chamber.
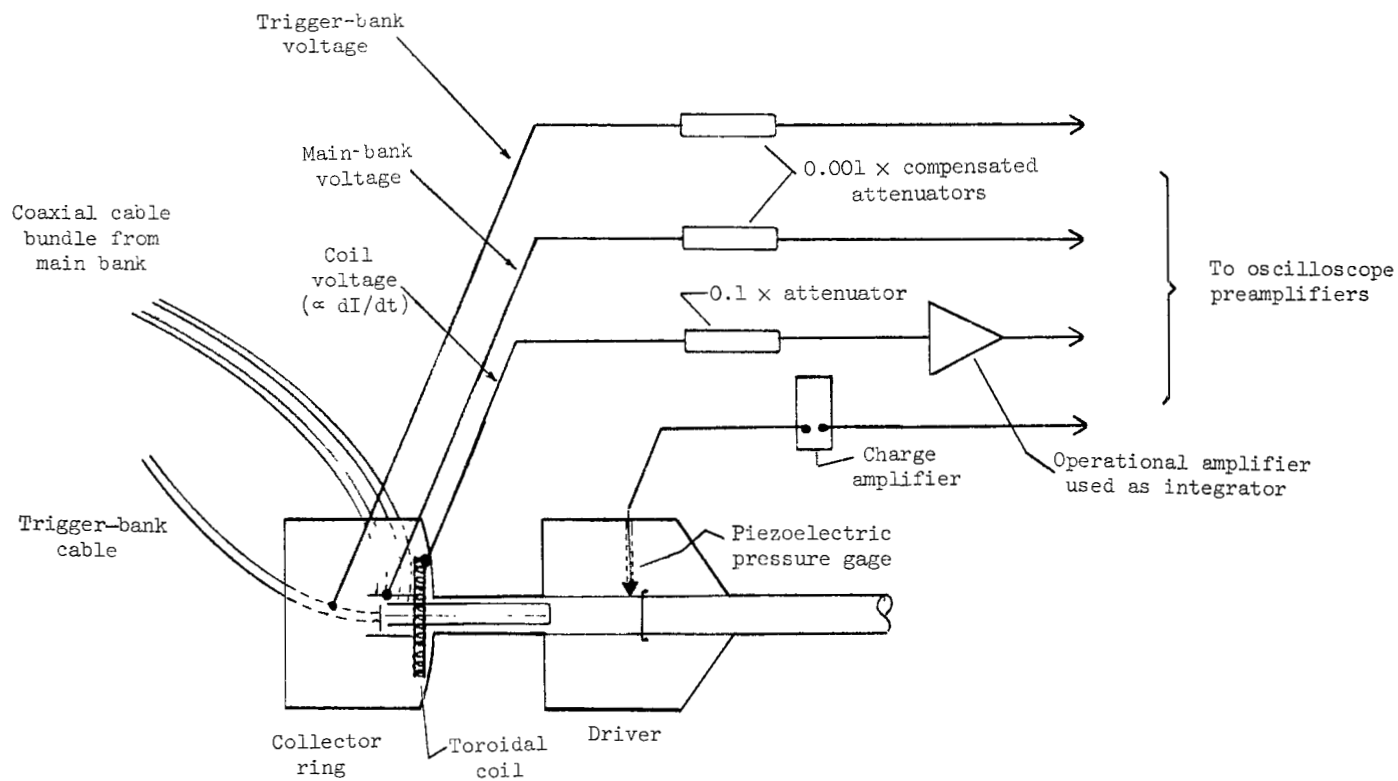
Figure 6.- Schematic drawing of instrumentation layout for monitoring arc-driver properties.

Voltage ↓  5 kV

→| |←

200 μsec

(a) Main-bank voltage.

Current ↓  1.04 MA

→| |←

200 μsec

(b) Current-coil output.

2760 N/cm$^2$

Pressure ↑

1380 N/cm$^2$

Time →

→| |←

200 μsec
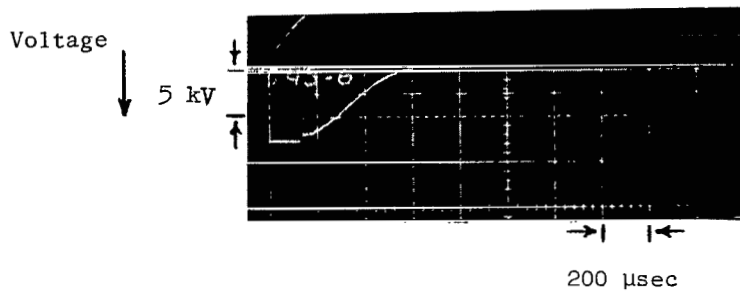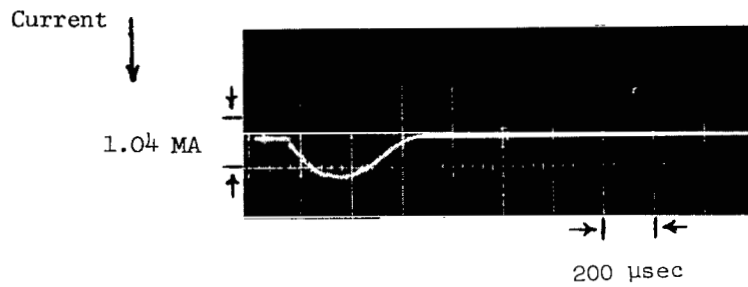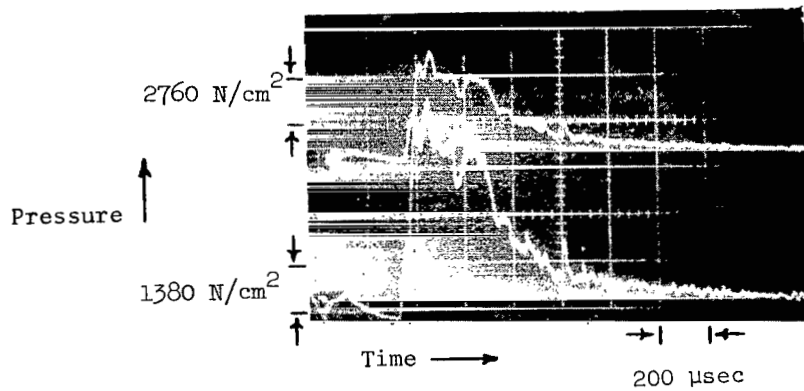
(c) Driver pressure-gage output.

Figure 7.- Sample oscilloscope records of driver properties
during discharge. One capacitor rack at 7.5 kV; driver
chamber gas, helium, at an initial pressure of 200 N/cm$^2$.

17
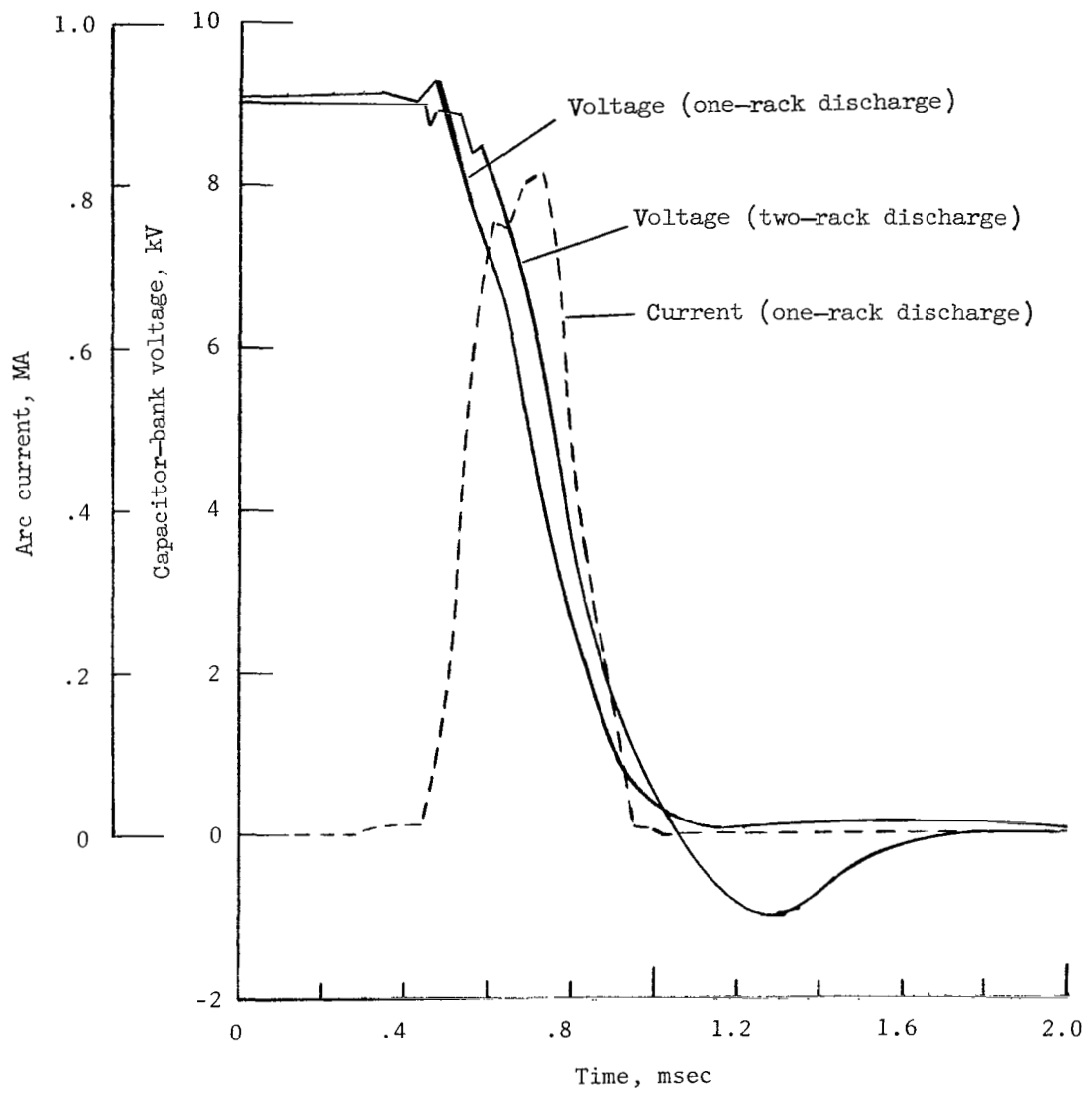
Figure 8.- Voltage and current histories for 9-kV discharges.
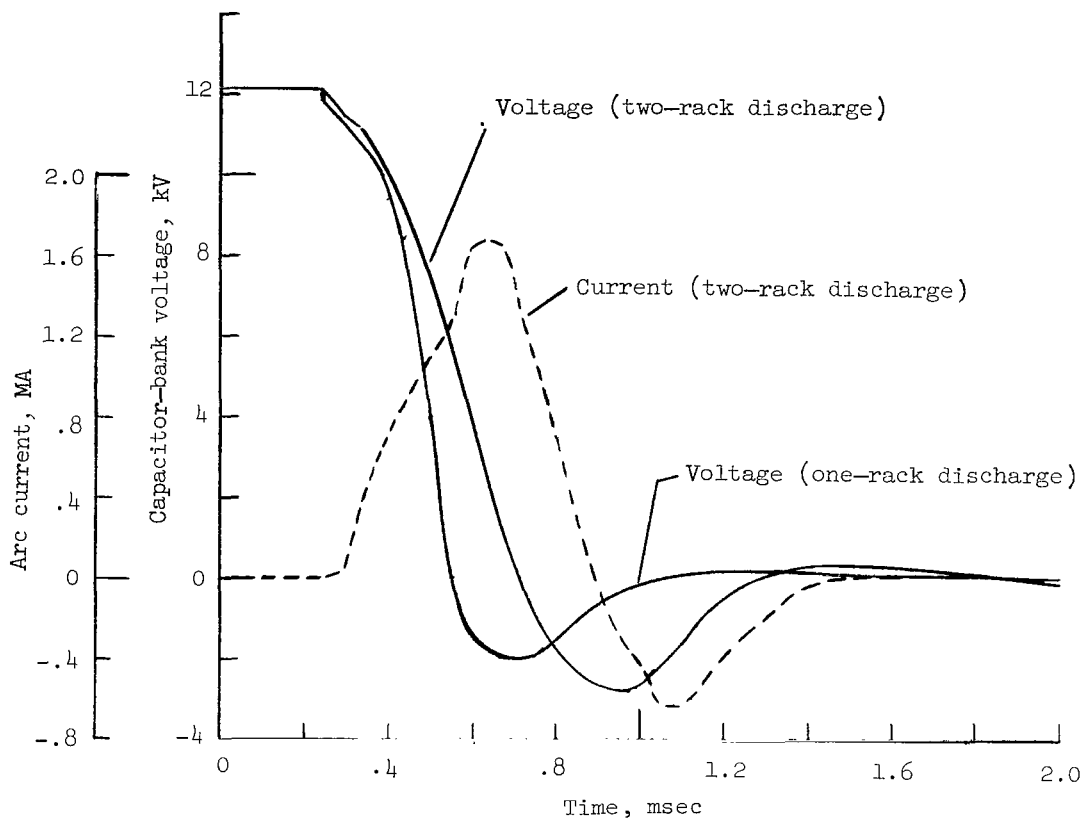
Figure 9.- Voltage and current histories for 12-kV discharges.
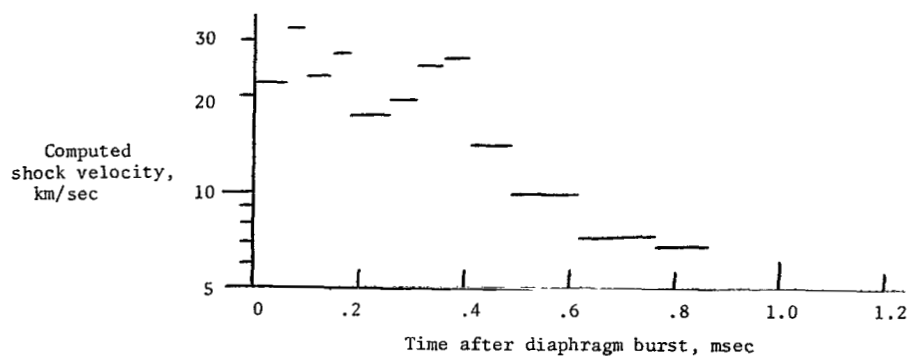
(a) Precursor ionization evident.
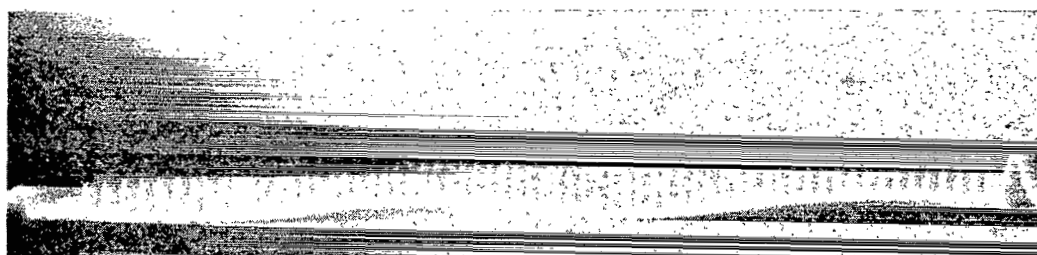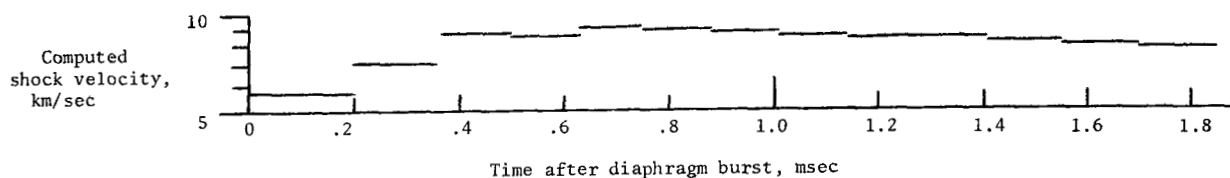


(b) Negligible effect from precursor ionization.

Figure 10.- Comparison of microwave signals for shock waves with and without evidence of precursor ionization. Shock velocities are computed from measurements over 5 cycles of the microwave signal; each bar represents 1.15 meters of shock travel. (Portions of a duplicate trace appear in the upper record.)
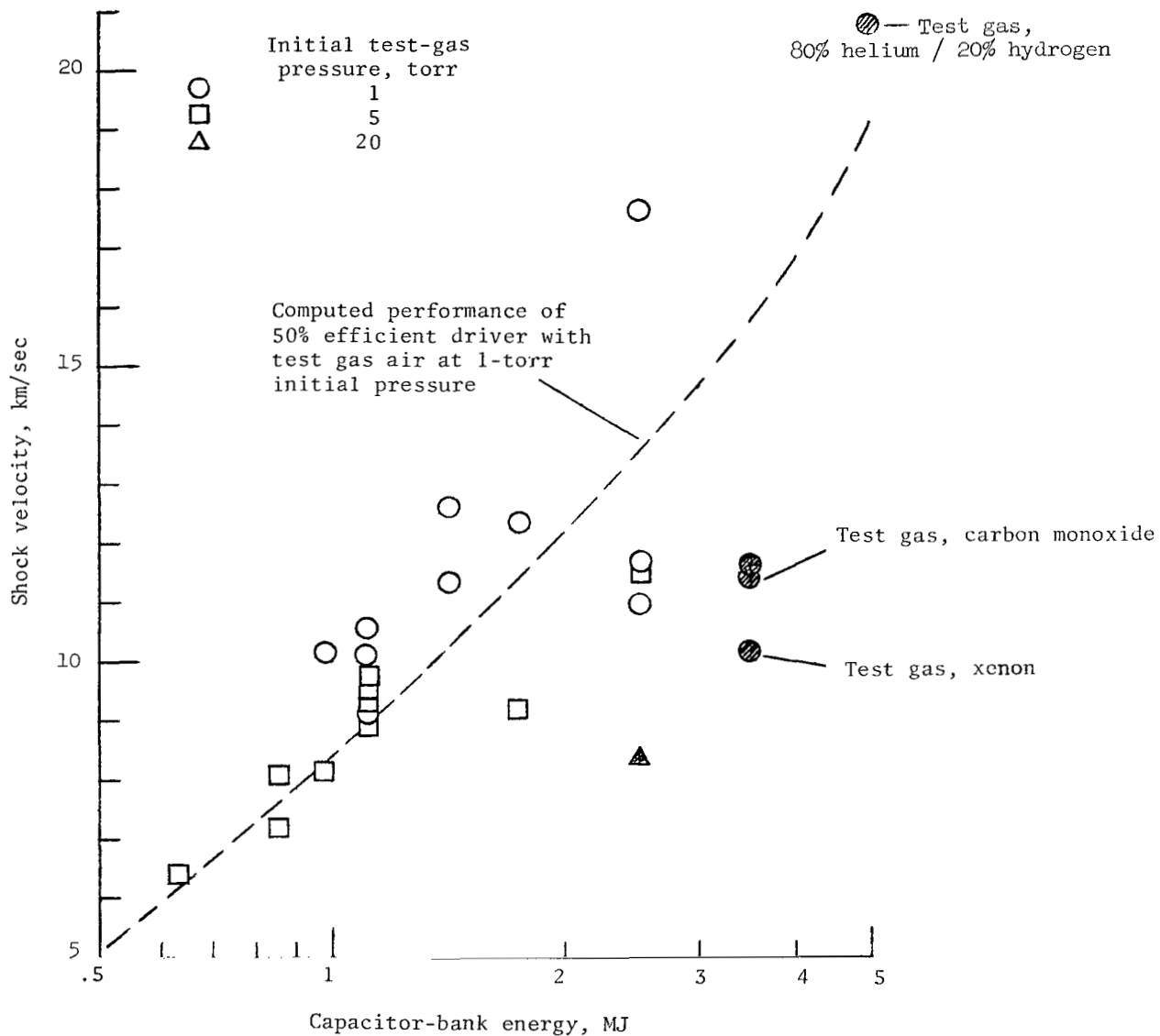
Figure 11.- Measured shock velocities as a function of initial capacitor-bank energy.
Test gas is air unless otherwise noted; shaded symbols indicate two-rack runs.
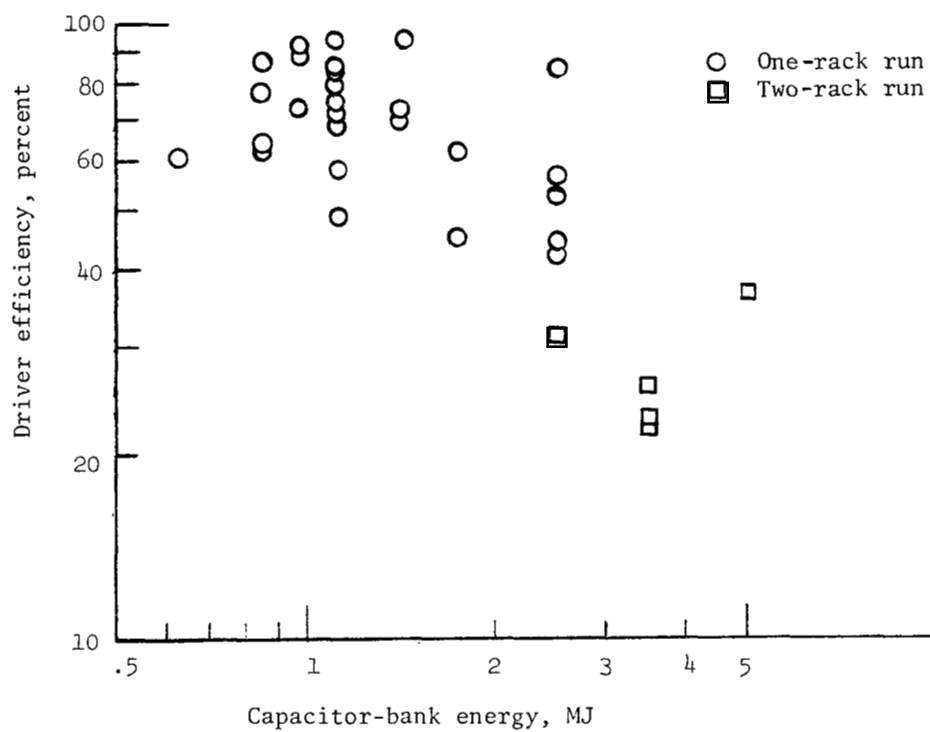
Figure 12.- Computed driver efficiencies as a function of
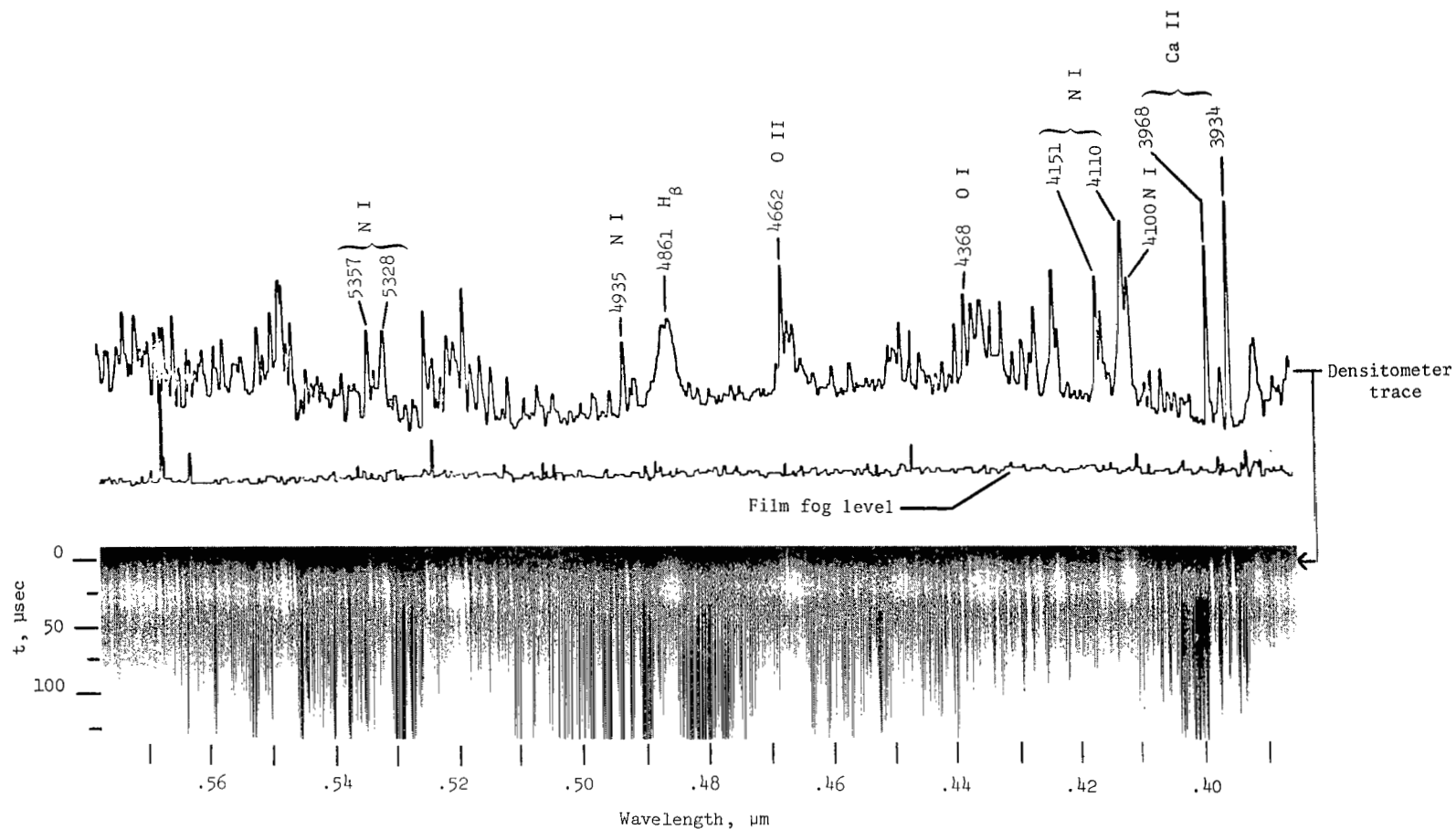initial capacitor-bank energy.
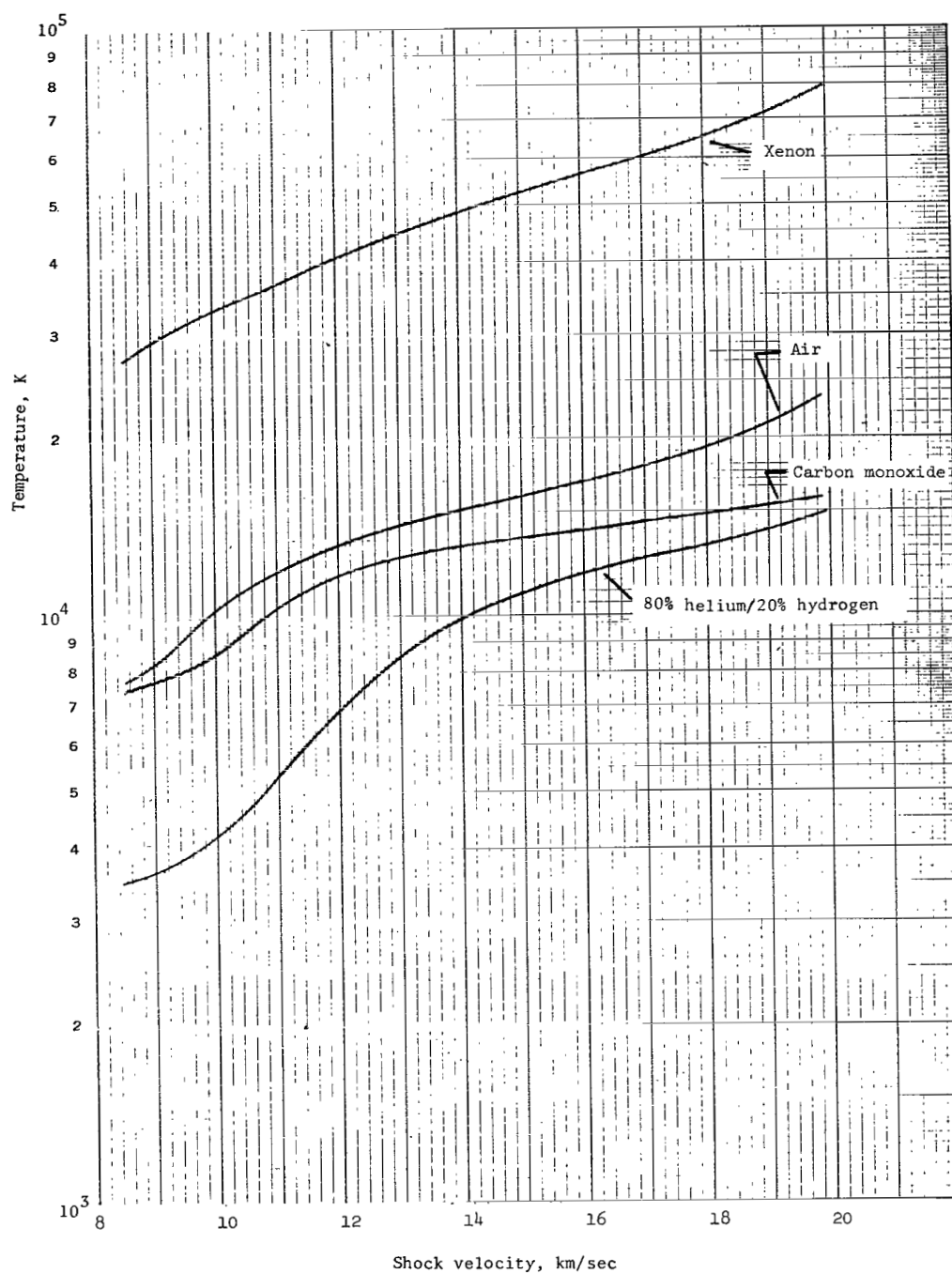
Figure 13.- Computed equilibrium temperature behind normal shock waves for test gases at initial ambient pressure of 1 torr.

(a) Test gas, air.  $p_1$ = 0.2 torr;  $V_S$ = 15.2 km/sec;  $T_{2,eq}$ = 14 700 K.

Figure 14.- Drum-camera spectrograms of incident-shock radiation for various test gases.  The wavelengths on the densitometer trace are in angstroms ($10^{-10}$ meter).  (Arrow at right indicates portion of film record where densitometer trace was made.)
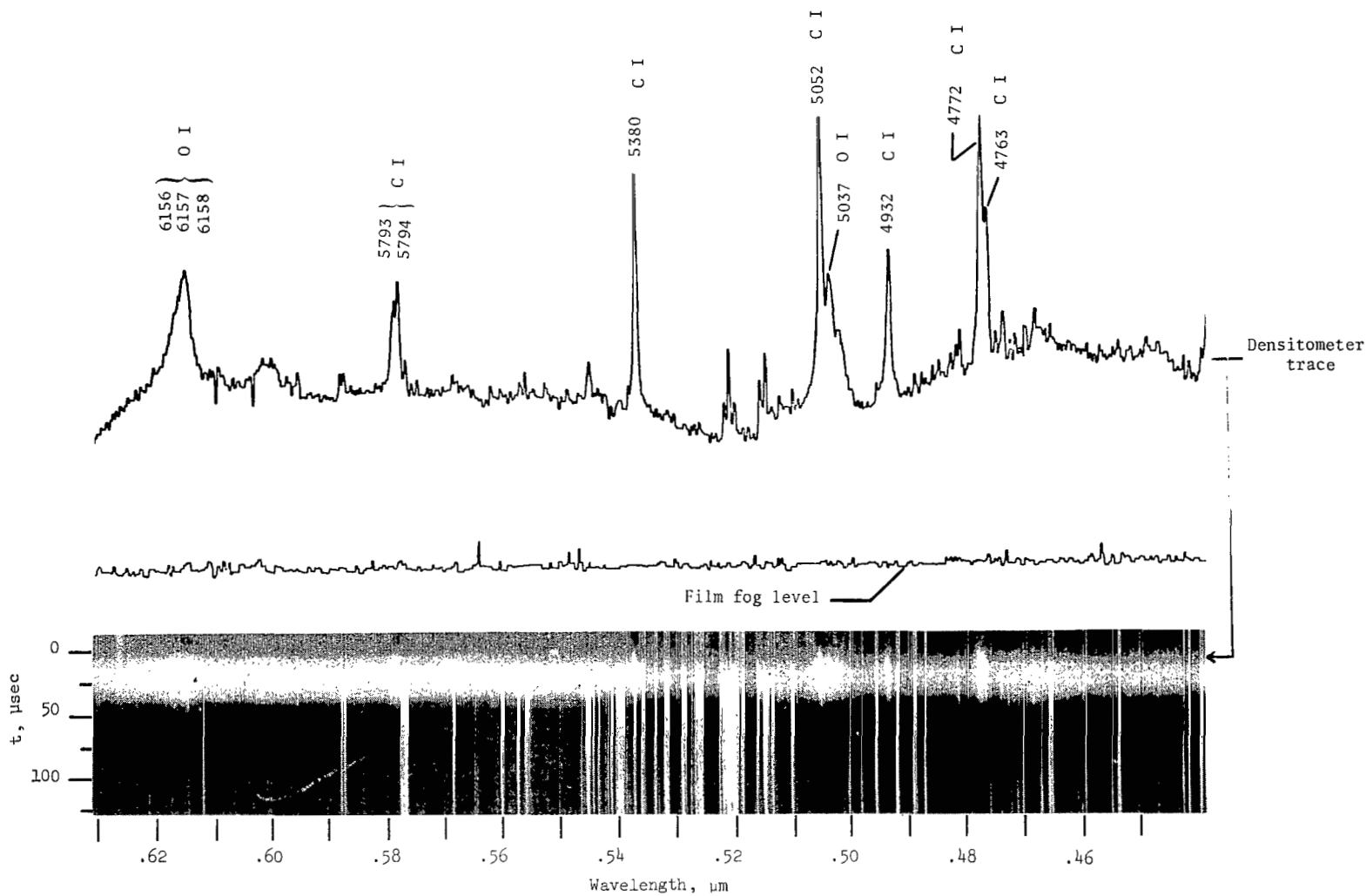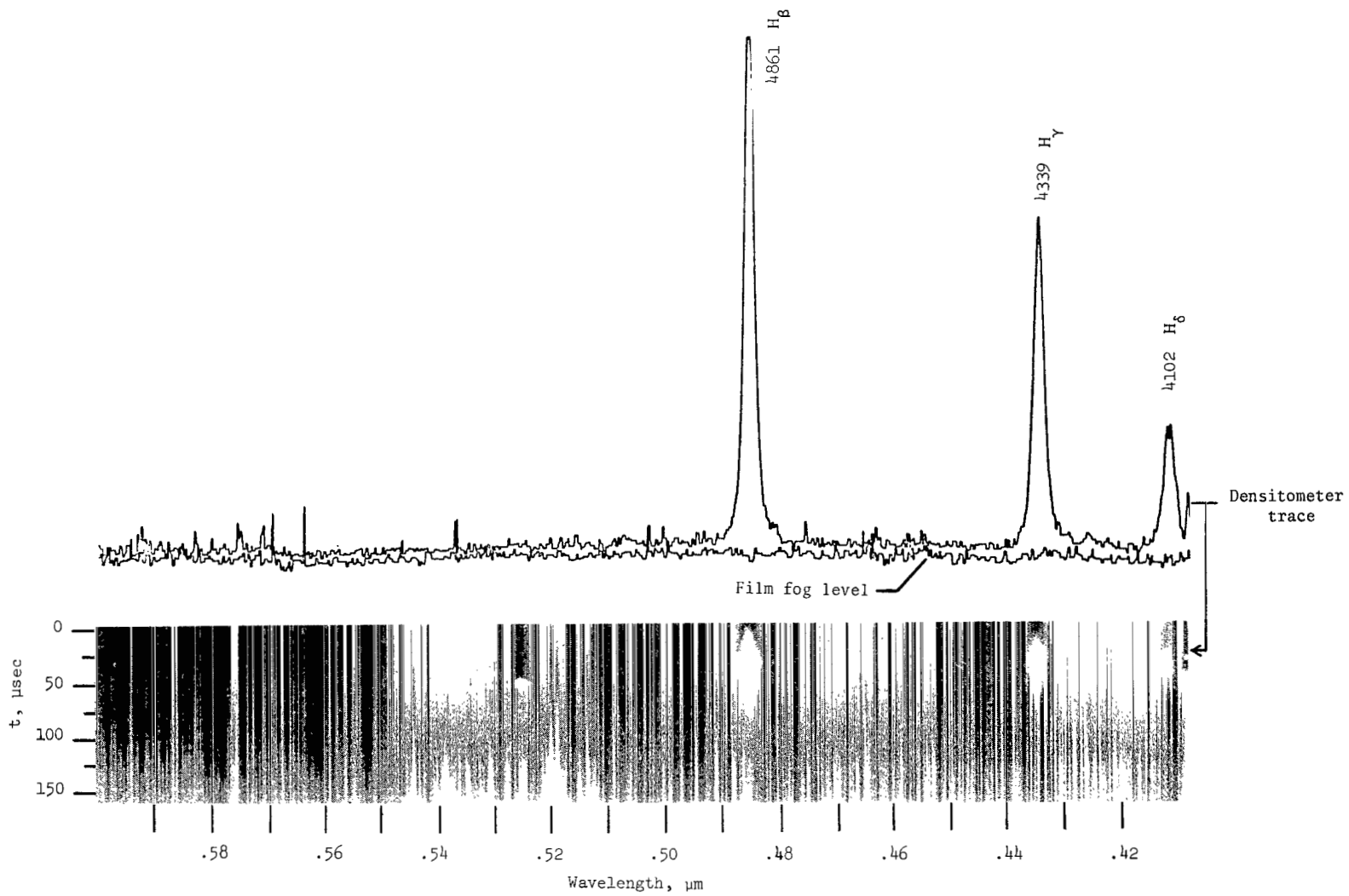
(b) Test gas, carbon monoxide. $p_1$ = 1 torr; $V_s$ = 11.4 km/sec; $T_{2,eq}$ = 11 000 K.

Figure 14.- Continued.
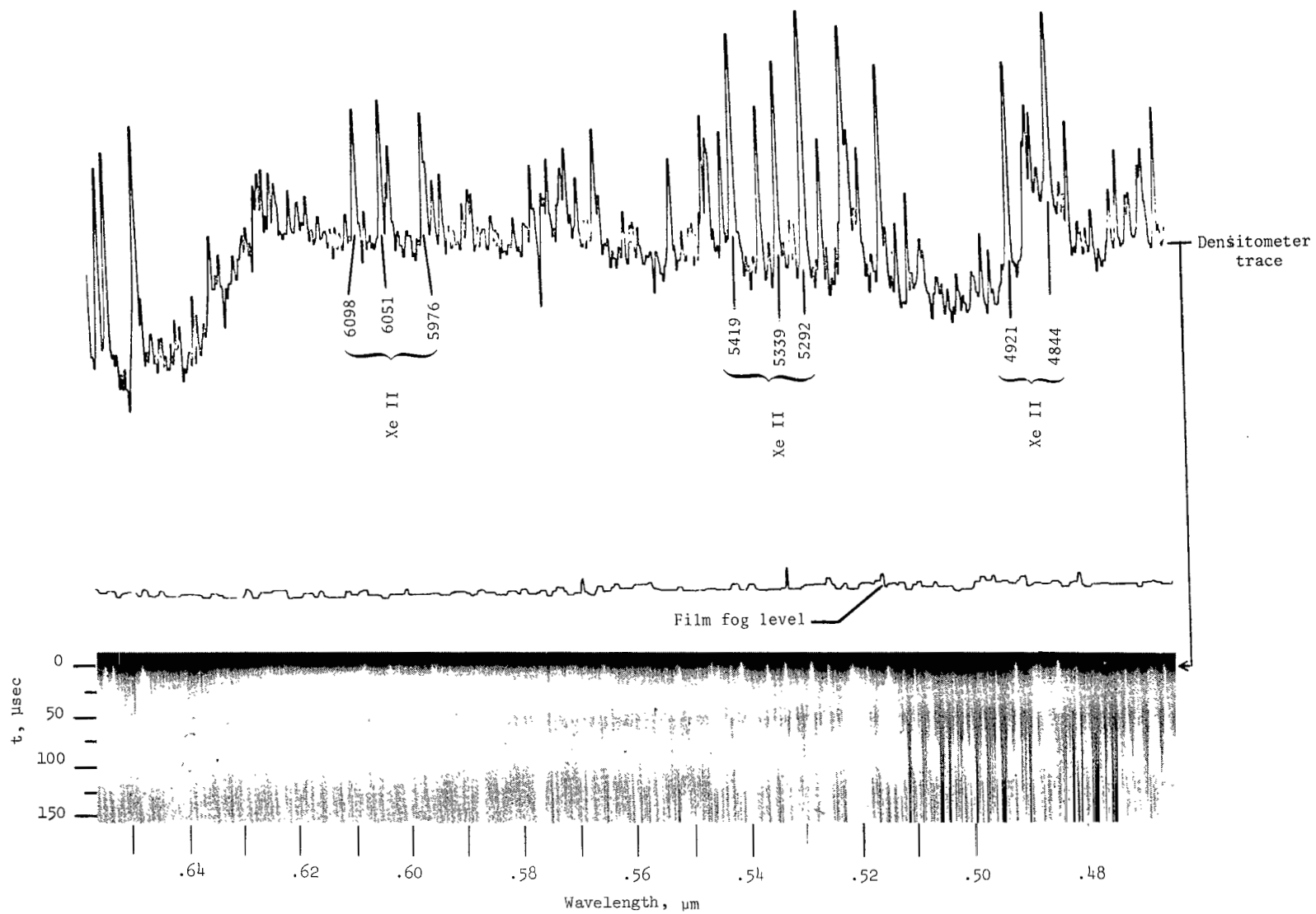
(c) Test gas, xenon.  $p_1$ = 1 torr;  $V_S$ = 10.2 km/sec;  $T_{2,eq}$ = 34 000 K.

Figure 14.- Continued.

(d) Test gas, 80-percent helium and 20-percent hydrogen.  $p_1$ = 1 torr;  $V_S$ = 20.8 km/sec;  $T_{2,eq}$ = 14 300 K.

Figure 14.- Concluded.

*"The aeronautical and space activities of the United States shall be conducted so as to contribute . . . to the expansion of human knowledge of phenomena in the atmosphere and space. The Administration shall provide for the widest practicable and appropriate dissemination of information concerning its activities and the results thereof."*

— NATIONAL AERONAUTICS AND SPACE ACT OF 1958

# NASA SCIENTIFIC AND TECHNICAL PUBLICATIONS

**TECHNICAL REPORTS:** Scientific and technical information considered important, complete, and a lasting contribution to existing knowledge.

**TECHNICAL NOTES:** Information less broad in scope but nevertheless of importance as a contribution to existing knowledge.

**TECHNICAL MEMORANDUMS:** Information receiving limited distribution because of preliminary data, security classification, or other reasons.

**CONTRACTOR REPORTS:** Scientific and technical information generated under a NASA contract or grant and considered an important contribution to existing knowledge.

**TECHNICAL TRANSLATIONS:** Information published in a foreign language considered to merit NASA distribution in English.

**SPECIAL PUBLICATIONS:** Information derived from or of value to NASA activities. Publications include conference proceedings, monographs, data compilations, handbooks, sourcebooks, and special bibliographies.

**TECHNOLOGY UTILIZATION PUBLICATIONS:** Information on technology used by NASA that may be of particular interest in commercial and other non-aerospace applications. Publications include Tech Briefs, Technology Utilization Reports and Technology Surveys.

*Details on the availability of these publications may be obtained from:*

## SCIENTIFIC AND TECHNICAL INFORMATION OFFICE

# NATIONAL AERONAUTICS AND SPACE ADMINISTRATION
Washington, D.C. 20546